

Dissipationless topological quantum computation for Majorana objects in the sparse-dense mixed encoding process

Ye-Min Zhan,^{1,2} Guan-Dong Mao^{1,2}, Yu-Ge Chen,³ Yue Yu,^{1,2,*} and Xi Luo^{4,†}

¹State Key Laboratory of Surface Physics, Fudan University, Shanghai 200433, China

²Department of Physics, Fudan University, Shanghai 200433, China

³Institute of Physics, Chinese Academy of Sciences, Beijing 100190, China

⁴College of Science, University of Shanghai for Science and Technology, Shanghai 200093, China



(Received 30 April 2024; revised 9 July 2024; accepted 29 July 2024; published 12 August 2024)

Topological quantum computation based on Majorana objects is subject to a significant challenge because at least some of the two-qubit quantum gates rely on the fermion (either charge or spin) parity of the qubits. This dependency renders the quantum operations involving these gates probabilistic when attempting to advance quantum processes within the quantum circuit model. Such an approach leads to significant information loss whenever measurements yield the undesired fermion parity. To resolve the problem of wasting information, we devise topological operations that allow for the nondissipative correction of information from undesired fermion parity to the desired one. We will use the sparse-dense mixed encoding process for the controlled-NOT gate as an example to explain how corrections can be implemented without affecting the quantum information carried by the computational qubits. This correction process can be applied to either the undesired input qubits or the fermion parity-dependent quantum gates, and it works for both Majorana-zero-mode-based and Majorana-edge-mode-based topological quantum computation.

DOI: [10.1103/PhysRevA.110.022609](https://doi.org/10.1103/PhysRevA.110.022609)

I. INTRODUCTIONS

The discovery of the topological state of matter has shed new light on designing the next generation of low-energy-consuming quantum electronic and spintronic devices [1–8]. Among these devices, the potential applications of topological quantum computation based on Majorana objects have attracted a lot of research interest. The study of Majorana physics in condensed matter physics stems from the Moore-Read wave function for the $\nu = 5/2$ even denominator fractional quantum Hall effect [9], or generally the p -wave superfluid/superconductor [10]. These Majorana objects obey non-Abelian statistics, which can be equivalently described by Majorana zero modes (MZMs) [11,12]. Following Kitaev's anyon-based fault-tolerant quantum computation proposal [13], the topological quantum gates, based on the MZMs and Majorana edge modes (MEMs) in the fractional quantum Hall effects, were designed [14–18].

Kitaev showed that MZMs can exist at the two ends of a topologically superconducting quantum chain [19]. These MZMs are exact realizations of those defined in [11,12,20]. Using the proximity effect of the s -wave superconductor/topological insulator interface, Fu and Kane also presented an effective model to realize the MZMs [21]. There are other proposals for MZMs, e.g., in semiconductor heterostructures [22], semiconductor-superconductor heterostructures [23], and so on [24–27]. Experimentally,

there have been many reports on MZMs emerging exactly in pairs [28–35]. Recently, evidence of MZMs has been reported on the surface of iron-based superconductors, where the pairs of MZMs are located on different surfaces that are separated by the topological bulk [36–41]. Braiding these MZMs is the central focus of the Majorana qubit manipulation, and there are mainly two ways to braid the MZMs: the real space or effective moving scheme [20,42–48] and the measurement-only scheme [49–56]. The initial step in the former approach involves the experimental confirmation of the MZMs' existence, a task that continues to pose significant challenges. The latter method, even for all Clifford gates, is not comprehensively understood. Recently, significant progress has been made in the designation of measurement-only Majorana qubits [57]. For example, a measurement-based realization of the Pauli gates and the controlled-Z (CZ) gate without ancillary qubits has been achieved. A new quantum computation process, based on fermion parity, is proposed as an alternative to the quantum circuit model [58].

The MEMs are characteristic of chiral topological superfluidity and superconductivity. Aside from that, in the $\nu = 5/2$ even denominator fractional quantum Hall state, the chiral edge states of Kitaev's spin liquid [59], the long-expected topological superconductor [4,5], and intrinsic time-reversal breaking chiral superconducting states in a topologically insulating thin film [60] are also regarded in the MEMs. In the s -wave superconductor/quantum anomalous Hall heterostructure, the proximity effect may induce a chiral topological superconducting phase [61,62]. Unfortunately, the experimental evidence of this scenario does not seem likely nowadays [63,64]. Thanks to the propagating property of the MEMs,

*Contact author: yuyue@fudan.edu.cn

†Contact author: xiluo@usst.edu.cn

we can understand the Majorana-based quantum gates well with the MEMs. Despite the experimental ambiguity, the theoretical studies for topological quantum computation with the MEMs are convenient [14–18,61,62]. In our recent work [65], we used MEMs in multilayers of the chiral superconductor thin film [66] to demonstrate that these MEMs can function as qubits for universal topological gates through their braidings. We also design quantum circuits and quantum devices for quantum computing processes, such as Shor’s integer factorization algorithm [65].

There are two distinct encoding methods for Majorana-based topological quantum computation. In sparse encoding, n logical qubits are realized using 2^n physical qubits. This method aligns closely with the quantum circuit model and offers significant reusability for quantum gates. However, its primary limitation is the inability to generate entangled states through braiding alone, necessitating the use of numerous auxiliary bits combined with measurements to achieve such states. On the other hand, dense encoding constructs an n -logical qubit system with $2n + 2$ physical qubits, inherently facilitating entanglement but encountering compatibility challenges with the tensor product structure inherent to the quantum circuit model. As the number of logical bits increases, a comprehensive redesign of all quantum gates becomes essential, negatively affecting the system’s reusability and scalability. Considering reusability and scalability, our recent work proposed a sparse-dense mixed encoding. Unlike solely relying on sparse encoding, this mixed encoding strategy eliminates the need for additional auxiliary qubits.

However, it was recognized that the braiding structures of some Majorana-based quantum gates are independent of the fermion parity (spin or charge) of the Majorana qubits; for example, most of the one-qubit gates and some direct product two-qubit gates. On the other hand, some of them are dependent on the fermion parity [51–56], such as the controlled-NOT (CNOT) gate, which is a key component in constructing the quantum circuit. The common way to deal with the fermion parity dependence of the quantum gates is to make a measurement with an ancillary qubit for the computational state. When the measured state has the desired fermion parity, the computational process continues, but when it does not have the desired parity, this input is abandoned. Although it was estimated that such abandonment is of acceptable efficiency in a real quantum computation process [65], it still wastes many resources.

Instead of such a probabilistic process, one may convert the undesired fermion spin-parity qubits to the desired one with some additional costs [55,56]. However, due to the use of sparse encoding [67], implementing the fermion spin-parity correction depends on two measurements. This causes the complexity of the computational process, as we will describe later. Furthermore, this correction operation cannot be applied to the sparse-dense mixed encoding in which we encode the qubits in [65]. The authors of Ref. [57] present a simpler operation that is relevant to converting the undesired outcome into the desired one for measurement-only topological quantum computation. It is argued that no ancillary qubit is required in the correction operation. These authors consider a hybrid of superconductor/two-dimensional topo-

logical insulator/ferromagnetic insulator where MZMs lie, and propose the deterministic Clifford gates.

In this work, we will study a correction operation for the fermion charge parity in the sparse-dense mixed encoding quantum computing process. We aim to improve our probabilistic quantum process in [65] to a deterministic one through an efficient fermion charge parity correction operation. In the sparse encoding sense, we also show that no additional ancillary qubit is required. Another way to resolve the problem of mismatched parity between the input qubits and the quantum gates is to correct the quantum gates, as briefly described in our previous work [65]. Here, we provide the specific process. By incorporating the correction process, we can achieve a dissipationless universal topological quantum computer. We discuss the efficiency of our process. Comparing with the correction process in [55,56], our process is more efficient.

This work is organized as follows: In Sec. II, we briefly summarize the main results of our previous work based on the sparse-dense encoding process [65]. We also review the fermion parity correction procedures provided in Ref. [56,57] for the sparse encoding. In Sec. III, we discuss the fermion charge parity correction for the sparse-dense mixed encoding in terms of our proposed quantum gates. The example for the dissipationless CNOT gate with the MEMs is explicitly implemented, in terms of the multilayers of the chiral superconductor thin film [65,66]. The efficiency of our computational process is estimated and compared with that of other processes.

II. MAJORANA QUBITS, FERMION PARITY, AND TOPOLOGICAL QUANTUM GATES

A. The basis

The quantum state space of the multi-Majorana objects is identical to the quantum states of the quantum Ising model [11,12]. According to Ivanov [12], Majorana fermions appear in pairs (γ_1, γ_2) with a phase difference $\pi/4$, namely, when they fuse, $\gamma_1^2 = \gamma_2^2 = 1$ but up to an overall phase $(\gamma_1, \gamma_2) \rightarrow \Psi_A \propto (\gamma_{A1} + i\gamma_{A2})/2$ or $\Psi_A^\dagger \propto (\gamma_{A1} - i\gamma_{A2})/2$, i.e., annihilating or creating a conventional fermion labeled as A with $\{\Psi_A, \Psi_A^\dagger\} = 1$, $\{\Psi_A, \Psi_A\} = \{\Psi_A^\dagger, \Psi_A^\dagger\} = 0$. The Pauli gates are X_A, Y_A, Z_A acting on the one-qubit for the basis $(|0_A\rangle, \Psi_A^\dagger|0_A\rangle)^T \equiv (|0_A\rangle, |1_A\rangle)^T$, called the Majorana one-qubit. The Majorana two-qubit gates are then defined in the basis of $(|00\rangle, \Psi_A^\dagger|00\rangle, \Psi_B^\dagger|00\rangle, \Psi_A^\dagger\Psi_B^\dagger|0\rangle)^T \equiv (|0_A0_B\rangle, |1_A0_B\rangle, |0_A1_B\rangle, |1_A1_B\rangle)^T$. The fermion charge parity of a quantum state is defined by $(-1)^F$, where F is the fermion number of the state. The fermion charge parity of the state $|0\rangle$ or $|1\rangle$ is ± 1 , while the states $(|0_A0_B\rangle, |1_A0_B\rangle, |0_A1_B\rangle, |1_A1_B\rangle)^T$ have $(-1)^F$ to be $(+, -, -, +)$. Notice that such a notion can also be applied to the spin system if identifying $|\downarrow\rangle \equiv |0\rangle$ and $|\uparrow\rangle \equiv |1\rangle$. In this case, the charge parity is replaced by the spin-parity [56].

For a particle number conserved system, the quantum state is characterized by F but not $(-1)^F$. But when fermions are created and annihilated in pairs, such as in superconductors, the conserved quantity is $(-1)^F$. In these systems, the Majorana one-qubit under the basis $(|0_A\rangle, |1_A\rangle)$ and Majorana two-qubits in the basis $(|0_A0_B\rangle, |1_A0_B\rangle, |0_A1_B\rangle, |1_A1_B\rangle)^T$ are

meaningless because of the fermion parity conservation. The minimal basis for a one-qubit is then $|\pm_{AB}\rangle_1$, where $|+\rangle_1 = (|0_A 0_B\rangle, |1_A 1_B\rangle)^T$ and $|-\rangle_1 = (|0_A 1_B\rangle, |1_A 0_B\rangle)^T$ with \pm referring to the fermion parity of the states. We have seen that most one-qubit gates are independent of the fermion parity of the basis (e.g., see [65]).

For the two-qubit gates, the dense encoding process takes the minimal basis with three pairs of Majorana objects [14,17,18],

$$\begin{aligned} |+\rangle_{ABC} &= (|0_A 0_B 0_C\rangle, |0_A 1_B 1_C\rangle, |1_A 0_B 1_C\rangle, |1_A 1_B 0_C\rangle)^T, \\ |-\rangle_{ABC} &= (|0_A 0_B 1_C\rangle, |0_A 1_B 0_C\rangle, |1_A 0_B 0_C\rangle, |1_A 1_B 1_C\rangle)^T. \end{aligned}$$

The two-qubits with the dense encoding are abbreviated as two-Dqubits.

B. One-qubit gates

There are two important kinds of elementary mutual braidings in the construction of the one-qubit gates in the fermion parity basis of Majorana objects. One is the braiding of Majorana fermions within a given fermion, say, R_{12} ($\gamma_{A1} \leftrightarrow \gamma_{A2}$), and the other one is the braiding of Majorana fermions between two different fermions, say B_{23} ($\gamma_{A2} \leftrightarrow \gamma_{B3}$). For MZMs, Ivanov [12] showed that in both parity even basis $|+\rangle_1$ and parity odd basis $|-\rangle_1$

$$R_{12} = \begin{pmatrix} e^{-i\pi/4} & 0 \\ 0 & e^{i\pi/4} \end{pmatrix}, \quad B_{23} = \frac{1}{\sqrt{2}} \begin{pmatrix} 1 & -i \\ -i & 1 \end{pmatrix}, \quad (1)$$

whereas the manipulation of moving the MZMs remains an experimental task.

In the following, we recall our one-qubit gates with the MEMs [61,62,65]. We describe the exchanging, braiding, and entangling of the MEMs in the parity basis $|\pm_{AB}\rangle_1$. Correspondingly, they are the exchanging, braiding, and fusion matrices in the unitary modular tensor category. In our scenario, the exchange operations act on γ_{1A}, γ_{2A} which are two MEMs from the same fermion Ψ_A and similarly for γ_{B3}, γ_{B4} . It was found that, in a seven-layered effective chiral superconductor, the MEMs $\gamma_{1,2}$ can be decomposed into a pair of Fibonacci anyons τ with conformal dimensions of $2/5$ and a pair of ε anyons with conformal dimensions of $1/10$ [66]. By denoting $G(\theta) = e^{i2\theta}$, then, through exchanging $\varepsilon_1, \varepsilon_2$ (or τ_1, τ_2) twice in γ_1 and γ_2 , both of γ_1 and γ_2 obtain a phase factor $G(\frac{\pi}{10}) = e^{i\frac{2\pi}{5}}$ [or $G(\frac{2\pi}{5}) = e^{i\frac{4\pi}{5}}$], while, exchanging each pair $\varepsilon_{1,2}$ and $\tau_{1,2}$ once, they obtain a phase factor $G(-\frac{\pi}{4})$ [65]. According to these phase factors, we can have the one-qubit phase gates $R_{12}(\theta/2) = \text{diag}(1, G(-\theta))$. Physically, this phase gate means that if the fermion number $n_A = 0$, nothing happens, and if $n_A = 1$, the fermion gains a phase $G(-\theta)$. It is easy to see that these phase gates are independent of the fermion parity of the basis. However, we find that $R_{34}^{(-)}(-\frac{\pi}{4})$ is not the same as $R_{34}^{(+)}(-\frac{\pi}{4})$ because $R_{34}^{(+)}(-\frac{\pi}{4}) = \text{diag}(1, i)$ while $R_{34}^{(-)}(-\frac{\pi}{4}) = \text{diag}(i, 1)$. These parity-dependent results are consistent with those in Ivanov [12], and they only differ by an overall constant phase. This parity dependency and its influence on designing the Majorana-based quantum device is not well considered in the literature, which is in fact the reason why multiqubit gates are dependent on the parity of the basis, and a parity correction process is needed. Later, we

will use the parity dependence of CNOT gate as an example and discuss the corresponding correction process.

The braiding gate B_{23} for γ_{2A} and γ_{3B} under the basis $|\pm_{AB}\rangle_1$ for the MEMs, proposed in [61,62], is not dependent on the fermion parity and is given by

$$B_{23} = \frac{1}{\sqrt{2}} \begin{pmatrix} i & 1 \\ 1 & i \end{pmatrix}. \quad (2)$$

This braiding process can be realized by the scattering of MEMs between a metal and a chiral topological superconductor, which is also topological [61,62,65] and easier than that of MZMs. And the Hadamard gate is given by

$$R_{12}\left(-\frac{\pi}{4}\right)B_{23}R_{12}\left(-\frac{\pi}{4}\right) = \frac{i}{\sqrt{2}} \begin{pmatrix} 1 & 1 \\ 1 & -1 \end{pmatrix} = iH. \quad (3)$$

With $H^{-1} = H$, one has

$$B_{23} = e^{-i\frac{\pi}{4}}HR_{12}\left(-\frac{\pi}{4}\right)H^{-1}.$$

This is the duality relation between fusion, exchange, and braiding in the unitary modular tensor category, $B = F^{-1}RF$, where $F = H^{-1} = H$ and $R = e^{-\frac{\pi}{4}}R_{12}$ [68]. Furthermore, we have $Z = [R_{12}(-\frac{\pi}{4})]^2$, $Y = (HZ)^2$, and

$$X = -iB_{23}^2 = -H\left[R_{12}\left(-\frac{\pi}{4}\right)\right]^2H. \quad (4)$$

The NOT gate X is given by braiding the MEM from Ψ_A and the MEM from Ψ_B twice. It is easy to check that $H, R_{12}(-\frac{\pi}{4})$, and B_{23} obey the pentagon and hexagon equations in the unitary modular tensor category [68].

Notice that $R_{12}(-\frac{\pi}{10})$ and $R_{12}(-\frac{2\pi}{5})$ do not belong to the Clifford gates [65]. Then, the quantum gates $\{H, R_{12}(-\frac{\pi}{4}), R_{12}(-\frac{\pi}{10}), \text{CNOT}\}$ form a universal set, and any elements of $SU(2)$ can be realized with desired precision [65,69]. We have also designed the corresponding devices for these gates with the multilayers of the chiral superconductor thin film [65]. For example, we recall the device designations for the Pauli gates X, Y, Z in Appendix A because they will play important roles in the fermion parity correction process.

C. Qubits and parity corrections in sparse encoding

In the sparse encoding process [67], four pairs of Majorana objects are considered for a two-qubit gate. Since there are eight basis states in a given fermion parity subspace, one has to choose four of them to span the computational space. We abbreviate such two-qubits as two-Squbits. In the computational process, because the mixing between the computational states and the noncomputational states cannot be avoided, the process either becomes probabilistic or needs to be corrected. As the cost of the fermion parity correction, an additional ancillary qubit, i.e., four Majorana objects, is introduced [55,56]. The advantage of the correction process in [56] is that, instead of the long-range braiding operation [55], only the local braidings are needed. On the other hand, besides introducing ancillary qubits, for the control-target two-qubit gates, both control and target qubits need to be corrected according to two measurements.

In the measurement-only process, Zhang *et al.* [57] proposed a scheme to correct the undesired outcome that arose

from the computational operation recently. In this model, the operations of fusion and braiding are effectively conducted through measurements rather than physically relocating Majorana fermions. However, these measurement processes can lead to the emergence of undesired quantum states. For example, they take the computational Squbit spanned by the basis

$$(|0_A 0_B 0_C 0_D\rangle, |0_A 0_B 1_C 1_D\rangle, |1_A 1_B 0_C 0_D\rangle, |1_A 1_B 1_C 1_D\rangle)^T. \quad (5)$$

The noncomputational basis, but with the same fermion parity, may be mixed with the computational basis due to the computational operations, and is

$$(|0_A 1_B 0_C 1_D\rangle, |0_A 1_B 1_C 0_D\rangle, |1_A 0_B 0_C 1_D\rangle, |1_A 0_B 1_C 0_D\rangle)^T. \quad (6)$$

Zhang *et al.* found that if one uses the parity correction operation to the Majorana one-qubit ($|0_{B,C}\rangle, |1_{B,C}\rangle$), i.e., $|0_{B,C}\rangle \leftrightarrow |1_{B,C}\rangle$, the noncomputational basis could be turned back to the computational one. Therefore, the required braiding operation can be completed correctly and deterministically. They further showed that, without adding an ancillary one-qubit, the correction operation could be realized by turning on the effective $X_{B,C}$ gates when the undesired parity is measured for the states at B, C according to the duality relation between the fusion, exchange, and braiding, that is, $X_{B,C} = F_{B,C}^{-1} R_{B,C}^2 F_{B,C}$, similar to Eq. (4).

D. Two-qubit gates in dense encoding

We recall the CNOT gate in the dense encoding [16,65]. We define $\Psi_A = (\gamma_{A1} + i\gamma_{A2})/2$, $\Psi_B = (\gamma_{B3} + i\gamma_{B4})/2$, and $\Psi_C = (\gamma_{C5} + i\gamma_{C6})/2$. Under the basis $|+_{ABC}\rangle_2$, the CNOT is given by

$$\begin{aligned} \text{CNOT}^{(+)} &= B_{45}^{(2)} R_{34}^{(2)} \left(-\frac{\pi}{4}\right) R_{56}^{(2)} \left(-\frac{\pi}{4}\right) B_{45}^{(2)} \\ &\quad \times R_{56}^{(2)} \left(-\frac{\pi}{4}\right) R_{34}^{(2)} \left(-\frac{\pi}{4}\right) R_{12}^{(2)-1} \left(-\frac{\pi}{4}\right) \\ &= \begin{pmatrix} 1 & 0 & 0 & 0 \\ 0 & 1 & 0 & 0 \\ 0 & 0 & 0 & 1 \\ 0 & 0 & 1 & 0 \end{pmatrix}, \end{aligned} \quad (7)$$

where the two-Dqubit gates $R_{12}^{(2)}(-\frac{\pi}{4}) = \text{diag}(1, 1, i, i)$, $R_{34}^{(2)}(-\frac{\pi}{4}) = \text{diag}(1, i, 1, i)$, and $R_{56}^{(2)}(-\frac{\pi}{4}) = \text{diag}(1, i, i, 1)$. $B_{45}^{(2)}$, as the counterpart of B_{23} , is given by

$$B_{45}^{(2)} = \frac{1}{\sqrt{2}} \begin{pmatrix} i & 1 & 0 & 0 \\ 1 & i & 0 & 0 \\ 0 & 0 & i & 1 \\ 0 & 0 & 1 & i \end{pmatrix}.$$

However, it is easy to see that the CNOT gate is dependent on the fermion parity. If we design the device according to the two-Dqubit gate sequence given by (7) in the parity odd basis $| -_{ABC}\rangle_2$, the result is not the right side of (7) [65]. The correct two-Dqubit gate sequence, which acts on $| -_{ABC}\rangle_2$ and gives the $\text{CNOT}^{(-)}$, is as follows:

$$\begin{aligned} \text{CNOT}^{(-)} &= B_{45}^{(2)} R_{34}^{(2)-1} \left(-\frac{\pi}{4}\right) R_{56}^{(2)} \left(-\frac{\pi}{4}\right) B_{45}^{(2)} \\ &\quad \times R_{56}^{(2)-1} \left(-\frac{\pi}{4}\right) R_{34}^{(2)} \left(-\frac{\pi}{4}\right) R_{12}^{(2)} \left(-\frac{\pi}{4}\right). \end{aligned} \quad (8)$$

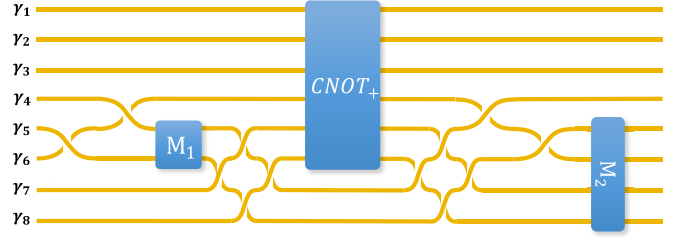


FIG. 1. The CNOT is in sparse encoding with even parity. The blue shaded area is the $\text{CNOT}^{(+)}$ in the dense encoding.

E. Qubits and universal topological quantum gates in the sparse-dense mixed encoding process

With three gates $\{H, Z^{\frac{1}{4}}, \text{CNOT}\}$, the quantum circuit models for quantum computation can be built [69,70]. To prove universality, the key essence is to create two orthogonal axes and a phase with an irrational number times π from the universal set, namely, any element in $SU(2)$ can be approximated with the desired precision. As mentioned before, the set of gates $\{H, \sqrt{Z}, R(-\frac{\pi}{10}), \text{CNOT}\}$ is universal [65]. Therefore, in principle, we can design the universal topological quantum computer. However, the dense encoding process is not directly relevant to a quantum circuit model. Therefore, we use the sparse-dense encoding process, i.e., taking the sparse encoding process to fit the quantum circuit model while processing the quantum computing by the dense encoding.

In our previous work [65], we started from the sparse encoding basis. To form a quantum circuit, we require each one-qubit to have the same fermion parity, say, $+$. Then two-Squbits are of the even fermion parity with the basis given by (5) and (6), denoted as $|+_{ABCD}\rangle_4$. The two-qubits are formed by four pairs of MEMS: $(\gamma_{A1}, \gamma_{A2})$, $(\gamma_{B3}, \gamma_{B4})$, $(\gamma_{C5}, \gamma_{C6})$, $(\gamma_{D7}, \gamma_{D8})$, and the initial input is enforced by $\gamma_{A1}\gamma_{A2}\gamma_{B3}\gamma_{B4} = -1$ and $\gamma_{C5}\gamma_{C6}\gamma_{D7}\gamma_{D8} = -1$. To reduce to dense encoding, we take $(\gamma_{4B}, \gamma_{5C})$ as the ancillary Majorana one-qubit. Before making the measurement M_1 , we entangle the first qubit and the second qubit with a series of exchanges and braiding, as shown in Fig. 1. If the measurement M_1 gives a positive fermion parity, then the rest of the MEMS propagate through the blue shaded area, which is a $\text{CNOT}^{(+)}$ in the dense encoding. The final step is measuring the output state. If M_2 gives $\gamma_{C5}\gamma_{C6}\gamma_{D7}\gamma_{D8} = -1$, this output state is the desired state ready for the next computational process. This is our quantum process for sparse-dense encoding.

The controlled-Y (CY) and CZ gates are obtained in terms of CNOT:

$$\text{CY} = R_{12} \left(-\frac{\pi}{4}\right) \text{CNOT} R_{12}^{-1} \left(-\frac{\pi}{4}\right),$$

$$\text{C}(iZ) = \text{CNOT} \cdot \text{CY}. \quad (9)$$

This means that these two-Dqubit gates are also dependent on the fermion parity.

III. THE FERMION PARITY CORRECTION FOR THE SPARSE-DENSE ENCODING PROCESS

As we have seen in the sparse-dense mixed encoding process, the input information will be abandoned when the

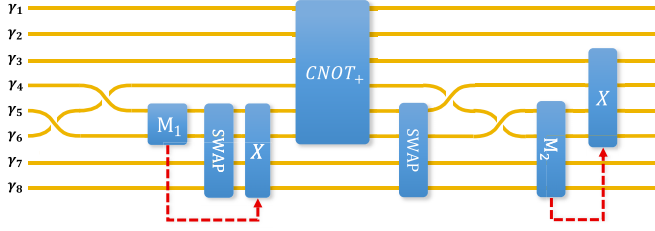


FIG. 2. Correcting the undesired fermion parity measured. M_1 and M_2 for the CNOT gate in the sparse-mixed encoding process.

undesired fermion parity is detected either in M_1 or M_2 . This makes the topological quantum computing process probabilistic. Although it has been estimated that this probabilistic process is still of good efficiency [65], vast quantum information resources are wasted. Similarly to the sparse encoding process [56,57], it is better to introduce the correction when the undesired fermion parity is detected. Two ways of the correction processes will be presented below, and they work for both MZM-based and MEM-based quantum computations.

A. Process I: Correcting the input qubits

As we have said, at a given A , the operation X_A switches the basis $|0_A\rangle \leftrightarrow |1_A\rangle$ and then exchanges the fermion parity of the basis. However, in the basis we take, there is no X_A operation. In our basis, the one-qubit space is spanned by $(|+\rangle_1) = (|0_A 0_B\rangle, |1_A 1_B\rangle)^T$ and $(|-\rangle_1) = (|0_A 1_B\rangle, |1_A 0_B\rangle)^T$. The $X = -iB_{23}^2$ gate does not change the fermion parity of the basis because $X(|0_A 0_B\rangle, |1_A 1_B\rangle)^T = (|1_A 1_B\rangle, |0_A 0_B\rangle)^T$ and $X(|0_A 1_B\rangle, |1_A 0_B\rangle)^T = (|1_A 0_B\rangle, |0_A 1_B\rangle)^T$. However, for a given A and B , we see that $|1_A\rangle \leftrightarrow |0_A\rangle$ and $|1_B\rangle \leftrightarrow |0_B\rangle$, i.e., $X = X_A \otimes X_B$.

We now show the details of the correction process for the CNOT gate. We have labeled four pairs of (γ_1, γ_2) , (γ_3, γ_4) , (γ_5, γ_6) , (γ_7, γ_8) as A, B, C, D . We take $\gamma_{4,5}$ as an ancillary qubit and measure its fermion parity, i.e., $i\gamma_4\gamma_5$. We label this measurement as M_1 in Fig. 2. If the measurement M_1 results in a positive fermion parity, we do nothing. For a negative fermion parity, i.e., an electron $\Psi_C^\dagger = (\gamma_C - i\gamma_5)/2$ being detected, the fermion parity correction can be operated as follows:

Since the total fermion parity is conserved, this means that the left two-Dqubits constituted by $\gamma_1, \gamma_2, \gamma_3, \gamma_6, \gamma_7, \gamma_8$ are also of the negative fermion parity. To correct this undesired fermion parity, let this electric signal switch on the gate X acting on the one-qubit constituted by $\gamma_{C4}, \gamma_{C5}, \gamma_{D7}, \gamma_{D8}$. This corresponds to braiding γ_{C8} and γ_{D4} twice (see []). Since $X = X_C \otimes X_D$, the fermion parity $i\gamma_{C4}\gamma_{C5}$ changes from $-$ to $+$ while $i\gamma_{D7}\gamma_{D8}$ also changes sign, and so $\gamma_1\gamma_2\gamma_3\gamma_6\gamma_7\gamma_8$ changes from $-$ to $+$. Therefore, the undesired fermion parity of the computational state in the dense encoding is corrected to the desired one.

We now describe how to make the measurement M_1 . If we choose the even fermion parity input state given by $\gamma_1\gamma_2\gamma_3\gamma_4 = \gamma_5\gamma_6\gamma_7\gamma_8 = -1$ [67], the corresponding computational two-Squbit basis is given by

$$(|0_A 0_B 0_C 0_D\rangle, |0_A 0_B 1_C 1_D\rangle, |1_A 1_B 0_C 0_D\rangle, |1_A 1_B 1_C 1_D\rangle)^T. \quad (10)$$

At this stage, measuring $i\gamma_4\gamma_5$ does not make sense because γ_4 and γ_5 do not form a fermion associated with the above basis. To get the fermion associated with that in the basis, let γ_6 exchange with $\gamma_{4,5}$ and form a new pair with γ_3 , and let (γ_4, γ_5) form another new pair (see Fig. 2). This is equivalent to applying $B_{45}B_{56}$ to the qubit $\{(\gamma_3, \gamma_4), (\gamma_5, \gamma_6)\}$ and results in a superposition of the computational and noncomputational two-Squbit basis

$$\begin{pmatrix} i|0_A 0_B 0_C 0_D\rangle + |0_A 1_B 1_C 0_D\rangle \\ -|0_A 0_B 1_C 1_D\rangle + i|0_A 1_B 0_C 1_D\rangle \\ |1_A 0_B 1_C 0_D\rangle + i|1_A 1_B 0_C 0_D\rangle \\ i|1_A 0_B 0_C 1_D\rangle - |1_A 1_B 1_C 1_D\rangle \end{pmatrix}, \quad (11)$$

where A, B, C, D label the Majorana fermion pairs $(\gamma_1, \gamma_2), (\gamma_3, \gamma_6), (\gamma_4, \gamma_5), (\gamma_7, \gamma_8)$.

We then measure $i\gamma_4\gamma_5$, i.e., performing M_1 in Fig. 2. When it is $+1$, the fermion number of the pair C is 0, and the basis (11) collapses to a two-Dqubit basis

$$(|0_A 0_B 0_D\rangle, |0_A 1_B 1_D\rangle, |1_A 1_B 0_D\rangle, |1_A 0_B 1_D\rangle)^T, \quad (12)$$

which is the basis of the two-qubits for the dense encoding in the even fermion parity.

When $i\gamma_4\gamma_5 = -1$, the fermion number of the pair C is 1, and the collapsed two-Dqubit basis is given by

$$(|0_A 1_B 1_C 0_D\rangle, -|0_A 0_B 1_C 1_D\rangle, |1_A 0_B 1_C 0_D\rangle, -|1_A 1_B 1_C 1_D\rangle)^T. \quad (13)$$

Here we introduce a quantum gate called the SWAP, which has the ability to exchange fermionic numbers between sites C and D , and is represented as follows:

$$\text{SWAP} = \frac{1}{\sqrt{2}} \begin{pmatrix} 1 & 0 & 0 & 0 \\ 0 & 0 & 1 & 0 \\ 0 & -1 & 0 & 0 \\ 0 & 0 & 0 & 1 \end{pmatrix}.$$

The braiding diagram for the SWAP operation is shown in Appendix C. Applying the SWAP to CD of (13),

$$(|0_A 1_B 1_C 0_D\rangle, |0_A 0_B 1_C 1_D\rangle, |1_A 0_B 1_C 0_D\rangle, |1_A 1_B 1_C 1_D\rangle)^T. \quad (14)$$

Notice that the overall phase of -1 has been omitted. Enacting $X_C \otimes X_D$ on this remaining basis, it becomes

$$(|0_A 1_B 0_C 1_D\rangle, |0_A 0_B 0_C 0_D\rangle, |1_A 0_B 0_C 1_D\rangle, |1_A 1_B 0_C 0_D\rangle)^T. \quad (15)$$

As we have said, this correction can be realized by braiding γ_5 and γ_7 twice, i.e., $B_{57}^2 \propto X = X_C \otimes X_D$, up to a total phase factor (see Fig. 2). This operation also switches the pair (γ_4, γ_5) from $i\gamma_4\gamma_5 = -1$ to 1. In the case of even parity, we also exchange the positions of C and D by employing the SWAP gate, and no additional phase is introduced.

The corrective approach is not unique. The basis (15) and that in (12) only differ by a linear transformation, which can be realized using a two-qubits gate. Another realization process and the definitions, and implementations of the SWAP, SWAP', and X gates are provided in the Appendices for reference.

Continuing the process and applying the CNOT⁽⁺⁾ gate, on the desired basis state (12), the output basis is given by

$$(|0_A 0_B 0_D\rangle, |0_A 1_B 1_D\rangle, |1_A 0_B 1_D\rangle, |1_A 1_B 0_D\rangle)^T$$

Putting the pair (γ_4, γ_5) with $i\gamma_4\gamma_5 = 1$ back, we have

$$(|0_A 0_B 0_C 0_D\rangle, |0_A 1_B 0_C 1_D\rangle, |1_A 0_B 0_C 1_D\rangle, |1_A 1_B 0_C 0_D\rangle)^T.$$

To complete this sparse-dense encoding process, we want to restore the input basis, i.e., perform the operations before the measurement M_2 . This means that we need to braid γ_6 with γ_4 and γ_5 again, and we then obtain the superposition state with $\gamma_1\gamma_2\gamma_3\gamma_4$ (and $\gamma_5\gamma_6\gamma_7\gamma_8$) either $= +1$ or $= -1$, i.e.,

$$\begin{pmatrix} |0_A 0_B 0_C 0_D\rangle + |0_A 1_B 1_C 0_D\rangle \\ |0_A 0_B 1_C 1_D\rangle + |0_A 1_B 0_C 1_D\rangle \\ |1_A 0_B 0_C 1_D\rangle + |1_A 1_B 1_C 1_D\rangle \\ |1_A 0_B 1_C 0_D\rangle + |1_A 1_B 0_C 0_D\rangle \end{pmatrix}. \quad (16)$$

We then measure $\gamma_5\gamma_6\gamma_7\gamma_8$, i.e., the measurement M_2 in Fig. 2(a). If it is -1 , we have the fermion parity even output basis in the sparse encoding,

$$(|0_A 0_B 0_C 0_D\rangle, |0_A 0_B 1_C 1_D\rangle, |1_A 1_B 1_C 1_D\rangle, |1_A 1_B 0_C 0_D\rangle)^T.$$

If the measurement M_2 is odd, we have the fermion parity odd output basis in the sparse encoding,

$$(|0_A 1_B 1_C 0_D\rangle, |0_A 1_B 0_C 1_D\rangle, |1_A 0_B 0_C 1_D\rangle, |1_A 0_B 1_C 0_D\rangle)^T.$$

We then enact $X = X_B \otimes X_C$ on the above output (see Fig. 2). The basis goes back to the computational basis (10).

This approach adjusts the fermion parity from an odd output basis to an even output basis, subsequently facilitating the implementation of a CNOT gate within sparse encoding. Without performing correction operations and discarding undesired states, the probability of achieving the correct outcome after N measurements is $\frac{1}{2^N}$. However, through corrections with a polynomial time complexity of $O(N)$, undesired states are transformed into desired states. This modification ensures that each result is deterministic, avoiding the exponentially decreased probability associated with uncorrected processes. It is noteworthy that, in contrast to the sparse encoding process described in [56], our method eliminates the need for additional ancillary qubits, a realization also achieved by [57] through a measurement-only scheme.

Furthermore, according to the above sparse-dense encoding process, any parity dependent two-Dqubit gate can be generalized to the two-Squbit gate in the same way because our process in fact does not specify the two-Dqubit gate. For a parity independent two-Dqubit gate, the fermion parity correction can be omitted after the measurement M_1 (see Fig. 4 in the Appendix).

Therefore, with the universal set of gates $\{H, \sqrt{Z}, R(-\frac{\pi}{10}), \text{CNOT}\}$, we can perform dissipationless universal topological quantum computation. In terms of sparse encoding, no additional ancillary qubit is needed for redundant measurements.

B. Process II: Correcting the gates in the dense encoding

As we mentioned in the previous work [65], we can also try to correct the parity-dependent gate if the measurement is undesired, instead of correcting the input data. For example, we start from the input as described in the last subsection. The braiding data of the CNOT gate in the sparse encoding is shown in Fig. 3(a), where the blue shade is the data of the

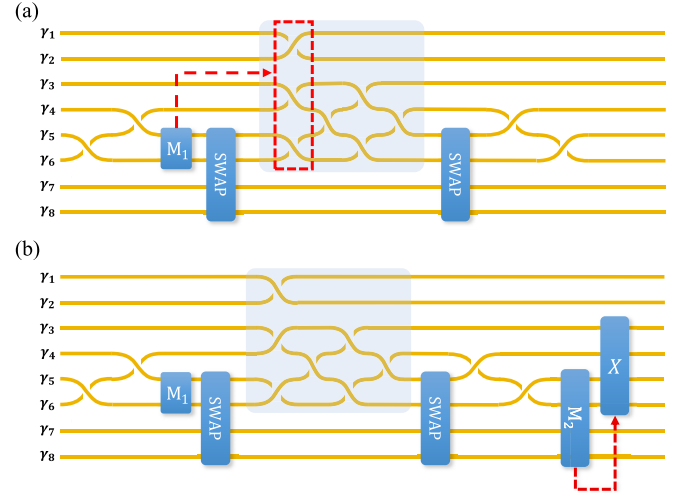


FIG. 3. Correcting the fermion-dependent gates. The blue transparent shade corresponds to the CNOT gate. (a) Before correction; (b) after correction.

CNOT⁽⁺⁾ for the dense encoding. We first do the measurement M_1 . If the result is positive fermion parity, we do nothing, as before. If the negative parity is detected, three signals are sent to three phase gates [see Fig. 3(a)]. These signals give orders so that the phase gates $R_{12}^{(2)-1}(-\frac{\pi}{4})$, $R_{34}^{(2)}(-\frac{\pi}{4})$, $R_{56}^{(2)}(-\frac{\pi}{4})$ turn to $R_{12}^{(2)}(-\frac{\pi}{4})$, $R_{34}^{(2)-1}(-\frac{\pi}{4})$, $R_{56}^{(2)-1}(-\frac{\pi}{4})$ and the CNOT⁽⁺⁾ \rightarrow CNOT⁽⁻⁾ [see Fig. 3(b)]. According to (7) and (8), this corrects the CNOT⁽⁺⁾ to the CNOT⁽⁻⁾. In practice, since $G(\mp\frac{\pi}{4}) = G(\pm\frac{\pi}{4})G(\pm\frac{\pi}{4})G(\pm\frac{\pi}{4})$, we do not reconstruct the exchange element when the undesired parity sign is received; instead, we turn on the other two same elements.

After applying the CNOT⁽⁻⁾ gate and restoring the pair (γ_4, γ_5) , we obtain

$$(|0_A 1_B 1_C 0_D\rangle, -|0_A 0_B 1_C 1_D\rangle, |1_A 1_B 1_C 1_D\rangle, -|1_A 0_B 1_C 0_D\rangle)^T.$$

Similarly to before, we revert to the input basis before measurement M_2 and obtain the superposition state

$$-i \begin{pmatrix} |0_A 0_B 0_C 0_D\rangle - |0_A 1_B 1_C 0_D\rangle \\ |0_A 0_B 1_C 1_D\rangle - |0_A 1_B 0_C 1_D\rangle \\ |1_A 0_B 0_C 1_D\rangle - |1_A 1_B 1_C 1_D\rangle \\ |1_A 0_B 1_C 0_D\rangle - |1_A 1_B 0_C 0_D\rangle \end{pmatrix}. \quad (17)$$

Finally, we perform M_2 and restore the output fermion parity to that of the input's parity [see Fig. 3(b)].

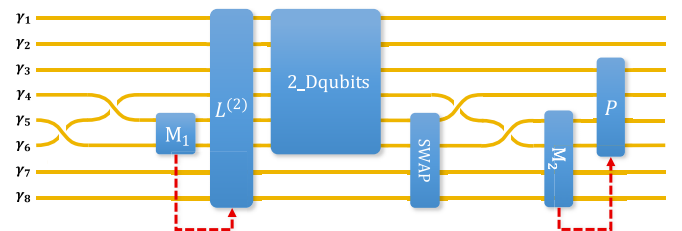


FIG. 4. Correcting the undesired fermion parity measured. $L^{(2)}$ is a possible linear transformation, and P is a Pauli gate to correct the undesired fermion parity.

C. Efficiency of the correction

Since our quantum process is dissipationless and topological in an ideal scenario, it is fault tolerant and very efficient when the temperature is low enough. We are not going to repeat the discussions on the possible error and efficiency of the general topological quantum computation processes [17,18,55,67]. Efficiency here means the number and complexity of the measurements, the signal sending, and the corrected gates.

As mentioned before, the manipulation of moving MZMs remains a difficult task. Therefore, we focus on the case of MEMs. In general, the time complexity (the number of quantum gates required) of the correction operation of the two processes we proposed, is $O(N)$, where N refers to the number of CNOT gates in the circuit. However, from the perspective of implementation, Process I is easier than Process II because the structure of the phase element $G(\frac{\pi}{4})$ in Process II is much more complicated than that of the X gate in Process I [65]. The former involves seven channels of chiral MEMs, and the interaction between the MEMs is specially manipulated, while the latter involves the exchange of two channels of free chiral MEMs, which can be easily done by the propagation of MEMs along the interface between chiral superconductor and normal metal [65].

Then we can evaluate the efficiency of implementing the CNOT gate. The study referenced in [56] presents a measurement-based approach for realizing the CNOT gate. According to this method, the execution of the CNOT gate involves three measurement operations alongside two quantum gates. In contrast, our proposed scheme necessitates only two measurements in addition to two quantum gate operations, with a time complexity that is comparable. However, the approach outlined in [56] necessitates the use of auxiliary qubits, which must be reinitialized following each measurement. This requirement results in a space complexity (pertaining to the computational resources consumed) of $O(N)$, where N represents the quantity of CNOT gates. Our methodology, on the other hand, does not demand extra auxiliary bits, thereby maintaining a space complexity of $O(1)$.

Subsequently, the efficiency of this scheme in realizing universal quantum computing can be analyzed. To achieve universal topological quantum computing, Ref. [55] chose to generate a magic state, which is simulated by adding noise and then purifying the quantum state. Their analysis reveals that, beyond the topological logic gates present in the quantum circuit, supplementary nontopological computational operations are essential for emulating a quantum circuit. The nontopological computational operations necessary to simulate a quantum circuit comprising L gates escalate to $O(L \ln L^3)$. In our case, the nontopological operation is a measurement, meaning the total number of nontopological computational operations present in our quantum circuit amounts to $O(N)$, where $N < L$ specifically refers to the count of CNOT gates rather than the total number of logic gates in [55].

Besides the above discussions on the efficiency and the common error shared with any topological quantum computing process [71], we discuss the efficiency of the charge detection in the measurements. In the measurements M_1 and M_2 , we need a charge-detecting meter to determine even or

odd fermion parity. In the literature, there are many proposals to design this kind of meter [51–53,72]. For example, Haack, Förster, and Büttiker designed a Mach-Zehnder interferometer coupled capacitively to two double quantum dots to detect the spin-parity of the two-qubit system [72]. The efficiency of the parity meter is given by the rate between the inverse of the time needed by the detector to distinguish the signal from the output noise [73,74] and the inverse of the coherence time of the measured quantum system.

Such a Mach-Zehnder interferometer is widely used in the two-dimensional electron gas in the quantum Hall regime with electron motion along edge states [75–80]. We consider the MEMs in the chiral superconductor which are similar to the chiral edge modes in quantum Hall effects. Thus, a similar efficiency study using the Mach-Zehnder interferometer may also be done to detect the fermion parity with M_1 and M_2 . We will leave the detailed designation of our parity meter and the calculation of the efficiency to further work.

IV. CONCLUSIONS

In conclusion, we have designed a set of dissipationless universal topological quantum gates with the MEMs in the chiral superconductor according to our fermion parity correction process and the probabilistic universal topological quantum gates designed in our previous work [65]. Our process may also be applied to the systems by directly moving the MZMs. Our process is more efficient than the existing parity correction process by saving the quantum information resource and reducing the number and complexity of measurements. There is also a correspondence between our process and the measurement-only scheme, and our study may inspire the universal gates, devices, and element designations for the measurement-only topological quantum computer.

ACKNOWLEDGMENT

We acknowledge useful discussions with Xin Liu. This work is supported by NNSF of China under Grant No. 12174067.

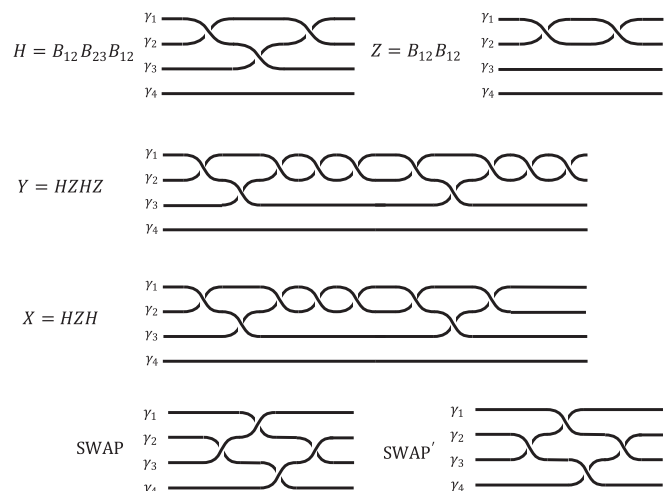


FIG. 5. Braiding diagrams for H , Z , Y , X , and SWAP gates.

APPENDIX A: GENERAL CORRECTIVE APPROACH

The corrective approach discussed above is not unique. For example, without using the SWAP gate in Fig. 2, after the measurement M_1 and the $X_C \otimes X_D$ operation, the basis becomes $(|0_A 1_B 0_C 1_D\rangle, -|0_A 0_B 0_C 0_D\rangle, |1_A 0_B 0_C 1_D\rangle, -|1_A 1_B 0_C 0_D\rangle)^T$. This basis and the one in (12) only differ by a linear transformation, which can be realized using a two-qubit gate such as the Y gate $Y^{(2)} = Y \oplus Y^T$, where $Y = HZH$ and $Y^T = ZHZH$ (see below). Another realization is to first apply $X = X_A \otimes X_B$, then apply $Z = Z_B \otimes Z_C$.

More generally, for any other two-qubit quantum gate that generates entangled states (two-qubits gate), one can always correct the undesired fermion parity using the general process

depicted in Fig. 4. Here, $L^{(2)}$ represents a linear transformation used to rectify the first measurement, while P denotes a Pauli gate employed to correct the undesired fermion parity observed in the second measurement.

APPENDIX B: BRAIDING DIAGRAMS OF QUANTUM GATES

In this Appendix, we show the braiding diagrams of the Pauli gates X, Y, Z and the SWAP gate in Fig. 5. The computational basis for two SWAP gate is $(|0_A 0_B\rangle, |0_A 1_B\rangle, |1_A 0_B\rangle, |1_A 1_B\rangle)^T$, and

$$\text{SWAP} = B_{32}B_{21}B_{43}B_{32} = \frac{1}{\sqrt{2}} \begin{pmatrix} 1 & 0 & 0 & 0 \\ 0 & 0 & 1 & 0 \\ 0 & -1 & 0 & 0 \\ 0 & 0 & 0 & 1 \end{pmatrix}, \quad \text{SWAP}' = B_{23}B_{12}B_{34}B_{23} = \frac{1}{\sqrt{2}} \begin{pmatrix} 1 & 0 & 0 & 0 \\ 0 & 0 & -1 & 0 \\ 0 & 1 & 0 & 0 \\ 0 & 0 & 0 & 1 \end{pmatrix}.$$

From the braiding diagrams, the corresponding designation of quantum gates can be realized by MEMs [65].

APPENDIX C: BRAIDING MATRIX

In the main text, we use braiding operations to obtain superposition states. Here, we present the complete matrices of the braiding operations under even parity. The computational basis used here is $(|0_A 0_B 0_C 0_D\rangle, |0_A 0_B 1_C 1_D\rangle, |0_A 1_B 0_C 1_D\rangle, |0_A 1_B 1_C 0_D\rangle, |1_A 0_B 0_C 1_D\rangle, |1_A 0_B 1_C 0_D\rangle, |1_A 1_B 0_C 0_D\rangle, |1_A 1_B 1_C 1_D\rangle)^T$; then the braiding operations are

$$(B_{45}B_{56})^+ = \frac{1}{\sqrt{2}} \begin{pmatrix} i & 0 & 0 & 1 & 0 & 0 & 0 & 0 \\ 0 & -1 & i & 0 & 0 & 0 & 0 & 0 \\ 0 & 1 & i & 0 & 0 & 0 & 0 & 0 \\ i & 0 & 0 & -1 & 0 & 0 & 0 & 0 \\ 0 & 0 & 0 & 0 & i & 0 & 0 & 1 \\ 0 & 0 & 0 & 0 & 0 & -1 & i & 0 \\ 0 & 0 & 0 & 0 & 0 & 1 & i & 0 \\ 0 & 0 & 0 & 0 & i & 0 & 0 & -1 \end{pmatrix},$$

$$(B_{65}B_{54})^+ = \frac{1}{\sqrt{2}} \begin{pmatrix} -1 & 0 & 0 & -1 & 0 & 0 & 0 & 0 \\ 0 & i & -i & 0 & 0 & 0 & 0 & 0 \\ 0 & -1 & -1 & 0 & 0 & 0 & 0 & 0 \\ -i & 0 & 0 & i & 0 & 0 & 0 & 0 \\ 0 & 0 & 0 & 0 & -1 & 0 & 0 & -1 \\ 0 & 0 & 0 & 0 & 0 & i & -i & 0 \\ 0 & 0 & 0 & 0 & 0 & -1 & -1 & 0 \\ 0 & 0 & 0 & 0 & -i & 0 & 0 & i \end{pmatrix}.$$

-
- [1] C. L. Kane and E. J. Mele, Z_2 Topological order and the quantum spin Hall effect, *Phys. Rev. Lett.* **95**, 146802 (2005).
[2] C. L. Kane and E. J. Mele, Quantum spin Hall effect in graphene, *Phys. Rev. Lett.* **95**, 226801 (2005).
[3] L. Fu, C. L. Kane, and E. J. Mele, Topological insulators in three dimensions, *Phys. Rev. Lett.* **98**, 106803 (2007).
[4] M. Z. Hasan and C. L. Kane, *Colloquium*: Topological insulators, *Rev. Mod. Phys.* **82**, 3045 (2010).
[5] X.-L. Qi and S.-C. Zhang, Topological insulators and superconductors, *Rev. Mod. Phys.* **83**, 1057 (2011).
[6] C.-Z. Chang *et al.*, Experimental observation of the quantum anomalous Hall effect in a magnetic topological insulator, *Science* **340**, 167 (2013).
[7] M. Gong, Y. Qian, M. Yan, V. W. Scarola, and C. Zhang, Dzyaloshinskii-Moriya interaction and spiral order in spin-orbit coupled optical lattices, *Sci. Rep.* **5**, 10050 (2015).
[8] M. Yan, Y. Qian, H.-Y. Hui, M. Gong, C. Zhang, and V. W. Scarola, Spin-orbit-driven transitions between Mott insulators and finite-momentum superfluids of bosons in optical lattices, *Phys. Rev. A* **96**, 053619 (2017).

- [9] G. Moore and N. Read, Nonabelions in the fractional quantum Hall effect, *Nucl. Phys. B* **360**, 362 (1991).
- [10] N. Read and D. Green, Paired states of fermions in two dimensions with breaking of parity and time-reversal symmetries and the fractional quantum Hall effect, *Phys. Rev. B* **61**, 10267 (2000).
- [11] C. Nayak and F. Wilczek, $2n$ -quasihole states realize 2^{n-1} -dimensional spinor braiding statistics in paired quantum Hall states, *Nucl. Phys. B* **479**, 529 (1996).
- [12] D. A. Ivanov, Non-Abelian statistics of half-quantum vortices in p -wave superconductors, *Phys. Rev. Lett.* **86**, 268 (2001).
- [13] A. Y. Kitaev, Fault-tolerant quantum computation by anyons, *Ann. Phys. (NY)* **303**, 2 (2003).
- [14] M. H. Freedman, A. Kitaev, M. J. Larsen, and Z. Wang, Topological quantum computation, *Bull. Am. Math. Soc.* **40**, 31 (2003).
- [15] L. S. Georgiev, Topologically protected gates for quantum computation with non-Abelian anyons in the Pfaffian quantum Hall state, *Phys. Rev. B* **74**, 235112 (2006).
- [16] L. S. Georgiev, *Lie Theory and Its Applications in Physics VII*, edited by V. K. Dobrev *et al.* (Heron, Sofia, 2008).
- [17] C. Nayak, S. H. Simon, A. Stern, M. Freedman, and S. Das Sarma, Non-Abelian anyons and topological quantum computation, *Rev. Mod. Phys.* **80**, 1083 (2008).
- [18] B. Field and T. Simula, Introduction to topological quantum computation with non-Abelian anyons, *Quantum Sci. Technol.* **3**, 045004 (2018).
- [19] A. Y. Kitaev, Unpaired Majorana fermions in quantum wires, *Phys. Usp.* **44**, 131 (2001).
- [20] J. Alicea, Y. Oreg, G. Refael, F. von Oppen, and M. P. A. Fisher, Non-Abelian statistics and topological quantum information, *Nat. Phys.* **7**, 412 (2011).
- [21] L. Fu and C. L. Kane, Superconducting proximity effect and Majorana fermions at the surface of a topological insulator, *Phys. Rev. Lett.* **100**, 096407 (2008).
- [22] J. D. Sau, R. M. Lutchyn, S. Tewari, and S. Das Sarma, Generic new platform for topological quantum computation using semiconductor heterostructures, *Phys. Rev. Lett.* **104**, 040502 (2010).
- [23] R. M. Lutchyn, J. D. Sau, and S. Das Sarma, Majorana fermions and a topological phase transition in semiconductor-superconductor heterostructures, *Phys. Rev. Lett.* **105**, 077001 (2010).
- [24] A. Yazdani, F. von Oppen, B. I. Halperin, and A. Yacoby, Hunting for Majoranas, *Science* **380**, eade0850 (2023).
- [25] Y. Tanaka, S. Tamura, and J. Cayao, Theory of Majorana zero modes in unconventional superconductors, *PTEP* **ptae065** (2024).
- [26] S. Takei, B. M. Fregoso, H.-Y. Hui, A. M. Lobos, and S. Das Sarma, Soft superconducting gap in semiconductor Majorana nanowires, *Phys. Rev. Lett.* **110**, 186803 (2013).
- [27] M. Barkeshli and J. D. Sau, Physical architecture for a universal topological quantum computer based on a network of Majorana nanowires, [arXiv:1509.07135](https://arxiv.org/abs/1509.07135).
- [28] V. Mourik, K. Zuo, S. M. Frolov, S. R. Plissard, E. P. A. M. Bakkers, and L. P. Kouwenhoven, Signatures of Majorana fermions in hybrid superconductor-semiconductor nanowire devices, *Science* **336**, 1003 (2012).
- [29] M. T. Deng, C. L. Yu, G. Y. Huang, M. Larsson, P. Caroff, and H. Q. Xu, Anomalous zero-bias conductance peak in a Nb–InSb nanowire–Nb hybrid device, *Nano Lett.* **12**, 6414 (2012).
- [30] A. Das, Y. Ronen, Y. Most, Y. Oreg, M. Heiblum, and H. Shtrikman, Zero-bias peaks and splitting in an Al–InAs nanowire topological superconductor as a signature of Majorana fermions, *Nat. Phys.* **8**, 887 (2012).
- [31] H. O. H. Churchill, V. Fatemi, K. Grove-Rasmussen, M. T. Deng, P. Caroff, H. Q. Xu, and C. M. Marcus, Superconductor-nanowire devices from tunneling to the multichannel regime: Zero-bias oscillations and magnetoconductance crossover, *Phys. Rev. B* **87**, 241401(R) (2013).
- [32] M. T. Deng, C. L. Yu, G. Y. Huang, M. Larsson, P. Caroff, and H. Q. Xu, Parity independence of the zero-bias conductance peak in a nanowire based topological superconductor-quantum dot hybrid device, *Sci. Rep.* **4**, 7261 (2014).
- [33] S. Nadj-Perge, Ilya K. Drozdov, J. Li, H. Chen, S. Jeon, J. Seo, A. H. MacDonald, B. A. Bernevig, and A. Yazdani, Observation of Majorana fermions in ferromagnetic atomic chains on a superconductor, *Science* **346**, 602 (2014).
- [34] J.-P. Xu, M.-X. Wang, Z. L. Liu, J.-F. Ge, X. J. Yang, C. H. Liu, Z. A. Xu, D. D. Guan, C. L. Gao, D. Qian, Y. Liu, Q.-H. Wang, F.-C. Zhang, Q.-K. Xue, and J.-F. Jia, Experimental detection of a Majorana mode in the core of a magnetic vortex inside a topological insulator-superconductor $\text{Bi}_2\text{Te}_3/\text{NbSe}_2$ heterostructure, *Phys. Rev. Lett.* **114**, 017001 (2015).
- [35] H. H. Sun *et al.*, Majorana zero mode detected with spin selective Andreev reflection in the vortex of a topological superconductor, *Phys. Rev. Lett.* **116**, 257003 (2016).
- [36] L. Kong *et al.*, Half-integer level shift of vortex bound states in an iron-based superconductor, *Nat. Phys.* **15**, 1181 (2019).
- [37] C. Chen, K. Jiang, Y. Zhang, C. Liu, Y. Liu, Z. Wang, and J. Wang, Atomic line defects and zero-energy end states in monolayer $\text{Fe}(\text{Te},\text{Se})$ high-temperature superconductors, *Nat. Phys.* **16**, 536 (2020).
- [38] Z. Wang, J. O. Rodriguez, L. Jiao, S. Howard, M. Graham, G. D. Gu, T. L. Hughes, D. K. Morr, and V. Madhavan, Evidence for dispersing 1D Majorana channels in an iron-based superconductor, *Science* **367**, 104 (2020).
- [39] C. Chen *et al.*, Quantized conductance of Majorana zero mode in the vortex of the topological superconductor $(\text{Li}_{0.84}\text{Fe}_{0.16})\text{OHFeSe}$, *Chin. Phys. Lett.* **36**, 057403 (2019).
- [40] P. Zhang *et al.*, Multiple topological states in iron-based superconductors, *Nat. Phys.* **15**, 41 (2019).
- [41] W. Liu *et al.*, A new Majorana platform in an Fe-As bilayer superconductor, *Nat. Commun.* **11**, 5688 (2020).
- [42] J. D. Sau, D. J. Clarke, and S. Tewari, Controlling non-Abelian statistics of Majorana fermions in semiconductor nanowires, *Phys. Rev. B* **84**, 094505 (2011).
- [43] B. van Heck, A. R. Akhmerov, F. Hassler, M. Burrello, and C. W. J. Beenakker, Coulomb-assisted braiding of Majorana fermions in a Josephson junction array, *New J. Phys.* **14**, 035019 (2012).
- [44] T. Hyart, B. van Heck, I. C. Fulga, M. Burrello, A. R. Akhmerov, and C. W. J. Beenakker, Flux-controlled quantum computation with Majorana fermions, *Phys. Rev. B* **88**, 035121 (2013).
- [45] X. J. Liu, C. L. M. Wong, and K. T. Law, Non-Abelian Majorana doublets in time-reversal-invariant topological superconductors, *Phys. Rev. X* **4**, 021018 (2014).

- [46] X. Liu, X. Li, D.-L. Deng, X.-J. Liu, and S. Das Sarma, Majorana spintronics, *Phys. Rev. B* **94**, 014511 (2016).
- [47] B. J. Brown and S. Roberts, Universal fault-tolerant measurement-based quantum computation, *Phys. Rev. Res.* **2**, 033305 (2020).
- [48] M. Brooks and C. Tahan, Quantum computation by spin-parity measurements with encoded spin qubits, *Phys. Rev. B* **108**, 035206 (2023).
- [49] R. Raussendorf and H. J. Briegel, A one-way quantum computer, *Phys. Rev. Lett.* **86**, 5188 (2001).
- [50] R. Raussendorf, D. E. Browne, and H. J. Briegel, Measurement-based quantum computation on cluster states, *Phys. Rev. A* **68**, 022312 (2003).
- [51] C. W. J. Beenakker, D. P. DiVincenzo, C. Emary, and M. Kindermann, Charge detection enables free-electron quantum computation, *Phys. Rev. Lett.* **93**, 020501 (2004).
- [52] H. A. Engel and D. Loss, Fermionic Bell-state analyzer for spin qubits, *Science* **309**, 586 (2005).
- [53] B. Trauzettel, A. N. Jordan, C. W. J. Beenakker, and M. Büttiker, Parity meter for charge qubits: An efficient quantum entangler, *Phys. Rev. B* **73**, 235331 (2006).
- [54] P. Bonderson, M. Freedman, and C. Nayak, Measurement-only topological quantum computation, *Phys. Rev. Lett.* **101**, 010501 (2008).
- [55] S. Bravyi, Universal quantum computation with the $\nu = 5/2$ fractional quantum Hall state, *Phys. Rev. A* **73**, 042313 (2006).
- [56] O. Zilberberg, B. Braunecker, and D. Loss, Controlled-NOT gate for multiparticle qubits and topological quantum computation based on parity measurements, *Phys. Rev. A* **77**, 012327 (2008).
- [57] S. Q. Zhang, J. S. Hong, Y. Xue, X. J. Luo, L. W. Yu, X. J. Liu, and X. Liu, Ancilla-free scheme of deterministic topological quantum gates for Majorana qubits, *Phys. Rev. B* **109**, 165302 (2024).
- [58] C. K. McLaughlan and B. Béri, Fermion-parity-based computation and its Majorana-zero-mode implementation, *Phys. Rev. Lett.* **128**, 180504 (2022).
- [59] A. Y. Kitaev, Anyons in an exactly solved model and beyond, *Ann. Phys. (NY)* **321**, 2 (2006).
- [60] X. Luo, Y. G. Chen, Z. Wang, and Y. Yu, Intrinsic chiral topological superconductor thin films, *Phys. Rev. B* **108**, 235147 (2023).
- [61] X.-L. Qi, T. L. Hughes, and S.-C. Zhang, Chiral topological superconductor from the quantum Hall state, *Phys. Rev. B* **82**, 184516 (2010).
- [62] B. Lian, X.-Q. Sun, A. Vaezi, X.-L. Qi, and S.-C. Zhang, Topological quantum computation based on chiral Majorana fermions, *Proc. Natl. Acad. Sci. USA* **115**, 10938 (2018).
- [63] W. J. Ji and X.-G. Wen, $\frac{1}{2}(e^2/h)$ conductance plateau without 1D chiral Majorana fermions, *Phys. Rev. Lett.* **120**, 107002 (2018).
- [64] M. Kayyalha, D. Xiao, R. X. Zhang, J. H. Shin, J. Jiang, F. Wang, Y.-F. Zhao, R. Xiao, L. Zhang, K. M. Fijalkowski, P. Mandal, M. Winnerlein, C. Gould, Q. Li, L. W. Molenkamp, M. H. W. Chan, N. Samarth, and C.-Z. Chang, Absence of evidence for chiral Majorana modes in quantum anomalous Hall-superconductor devices, *Science* **367**, 64 (2020).
- [65] Y. M. Zhan, Y. G. Chen, B. Chen, Z. Q. Wang, Y. Yu, and X. Luo, Universal topological quantum computation with strongly correlated Majorana edge modes, *New J. Phys.* **24**, 043009 (2022).
- [66] Y. C. Hu and C. L. Kane, Fibonacci topological superconductor, *Phys. Rev. Lett.* **120**, 066801 (2018).
- [67] S. D. Sarma, M. Freedman, and C. Nayak, Majorana zero modes and topological quantum computation, *npj Quantum Inf.* **1**, 15001 (2015).
- [68] G. Moore and N. Seiberg, Classical and quantum conformal field theory, *Commun. Math. Phys.* **123**, 177 (1989).
- [69] P. O. Boykin, T. Mor, M. Pulver, V. Roychowdhury, and F. Vatan, A new universal and fault-tolerant quantum basis, *Inf. Process. Lett.* **75**, 101 (2000).
- [70] A. Barenco, C. H. Bennett, R. Cleve, D. P. DiVincenzo, N. Margolus, P. Shor, T. Sleator, J. A. Smolin, and H. Weinfurter, Elementary gates for quantum computation, *Phys. Rev. A* **52**, 3457 (1995).
- [71] S. Das Sarma, M. Freedman, and C. Nayak, Topologically protected qubits from a possible non-Abelian fractional quantum Hall state, *Phys. Rev. Lett.* **94**, 166802 (2005).
- [72] G. Haack, H. Förster, and M. Büttiker, Parity detection and entanglement with a Mach-Zehnder interferometer, *Phys. Rev. B* **82**, 155303 (2010).
- [73] A. N. Korotkov, Continuous quantum measurement of a double dot, *Phys. Rev. B* **60**, 5737 (1999).
- [74] M. Büttiker, Scattering theory of current and intensity noise correlations in conductors and wave guides, *Phys. Rev. B* **46**, 12485 (1992).
- [75] Y. Ji, Y. Chung, D. Sprinzak, M. Heiblum, D. Mahalu, and H. Shtrikman, An electronic Mach-Zehnder interferometer, *Nature (London)* **422**, 415 (2003).
- [76] I. Neder, M. Heiblum, Y. Levinson, D. Mahalu, and V. Umansky, Unexpected behavior in a two-path electron interferometer, *Phys. Rev. Lett.* **96**, 016804 (2006).
- [77] P. Roulleau, F. Portier, D. C. Glatli, P. Roche, A. Cavanna, G. Faini, U. Gennser, and D. Mailly, Direct measurement of the coherence length of edge states in the integer quantum Hall regime, *Phys. Rev. Lett.* **100**, 126802 (2008).
- [78] L. V. Litvin, A. Helzel, H.-P. Tranitz, W. Wegscheider, and C. Strunk, Edge-channel interference controlled by Landau level filling, *Phys. Rev. B* **78**, 075303 (2008).
- [79] E. Bieri, M. Weiss, O. Göktas, M. Hauser, C. Schönenberger, and S. Oberholzer, Finite-bias visibility dependence in an electronic Mach-Zehnder interferometer, *Phys. Rev. B* **79**, 245324 (2009).
- [80] P. Roulleau, F. Portier, P. Roche, A. Cavanna, G. Faini, U. Gennser, and D. Mailly, Tuning decoherence with a voltage probe, *Phys. Rev. Lett.* **102**, 236802 (2009).